ELSEVIER

Composites: Part B 31 (2000) 77–86

composites
Part B: engineering

www.elsevier.com/locate/compositesb

Modeling of progressive damage in aligned and randomly oriented discontinuous fiber polymer matrix composites☆

H.K. Lee*, S. Simunovic

Computer Science and Mathematics Division, Oak Ridge National Laboratory, Oak Ridge, TN 37831-6359, USA

Received 1 November 1999; accepted 8 December 1999

Abstract

Damage constitutive models based on micromechanical formulation and a combination of micromechanical and macromechanical damage criterions are presented to predict progressive damage in aligned and random fiber-reinforced composites. Progressive interfacial fiber debonding models are considered in accordance with a statistical function to describe the varying probability of fiber debonding. Based on an effective elastoplastic constitutive damage model for aligned fiber-reinforced composites, micromechanical damage constitutive models for two- and three-dimensional (2D and 3D) random fiber-reinforced composites are developed. The constitutive relations and overall yield function for aligned fiber orientations are averaged over all orientations to obtain the constitutive relations and overall yield function of 2D and 3D, random fiber-reinforced composites. Finally, the present damage models are implemented numerically and compared with experimental data to show the progressive damage behavior of random fiber-reinforced composites. Furthermore, the damage models will be implemented into a finite element program to illustrate the dynamic inelastic behavior and progressive crushing in composite structures under impact loading. Published by Elsevier Science Ltd.

Keywords: Damage constitutive models

1. Introduction

Damage and failure modes in discontinuous fiber composites having a complex structure are best understood in terms of the arrangement of reinforcing fibers and matrix resin. Analyses and tests to assess the damage in these composites have been carried out [1–4]. The different failure mechanisms of laminate composites caused by stresses in fiber direction or perpendicular to the reinforcement have been cast into failure criteria based on experimental evidence by a number of researchers [5–7]. However, new failure criteria based on experimental verifications are needed for performing failure analysis of discontinuous, aligned and random fiber composites, because the failure mechanisms of discontinuous fiber composites are different from those for laminates. A more detailed failure review of fiber-reinforced composites can be found in Matzenmiller and Schweizerhof [8], Kutlu and Chang [9], Meraghni and Benzeggagh [10], and Meraghni et al. [11].

Micromechanical approaches enable us to evaluate and predict local stress and strain fields in each constituent. In addition, these approaches allow us to address local fluctuations due to the onset and the evolution of damage mechanisms. Therefore, the derivation of the constitutive Equations in the form of a phenomenological parameter model from entirely micromechanical considerations is required to perform the rigorous analysis of composite structures. Such an approach is more justified in the case of composite materials reinforced with randomly oriented discontinuous fibers. Indeed, the microstructure of these materials, the complexity of damage mechanisms, and the diversity of their damage scenarios significantly influence their overall properties. Furthermore, because of the natural tendency of the structure to acquire lower energy modes, both material and structural damage processes need to be thoroughly understood and modeled to simulate and eventually design the desirable sustained crush of the component. Therefore, accurate analysis and the ability to simulate the complete response of components and systems of random fiber polymer matrix composites are essential and require accurate micromechanical damage constitutive models.

☆ This manuscript has been authored by a contractor of the US Government under contract no. DE-AC05-96OR22464. Accordingly, the US Government retains a nonexclusive, royalty-free license to publish or reproduce the published form of this contribution, or allow others to do so, for US Government purposes.

* Corresponding author. Tel.: + 1-423-574-4837; fax: + 1-423-574-7463.

E-mail address: leeh@ornl.gov (H.K. Lee).

1359-8368/00/$ - see front matter Published by Elsevier Science Ltd.
PII: S1359-8368(99)00070-0

A micromechanical analysis based on the modified Mori–Tanaka method was performed by Meraghni and Benzeggagh [10] and Meraghni et al. [11] to address the effect of matrix degradation and interfacial debonding on stiffness reduction in a random discontinuous fiber composite. Their modeling relied on an experimental approach, developed through a methodology of experimental identification of basic damage mechanisms, which involved amplitude analysis of acoustic emission and microscopic observations. Tohgo and Weng [12] and Zhao and Weng [13–15] proposed progressive interfacial damage models for ductile matrix composites. They used Weibull's [16] probability distribution function to describe the probability of particle debonding. Ju and Lee [17] developed a micromechanical damage model to predict the overall elastoplastic behavior and damage evolution in ductile matrix composites. In their derivation, to estimate the overall elastoplastic-damage behavior, an effective yield criterion was derived based on the ensemble-volume averaging procedure and the first-order effects of eigen-strains stemming from the existence of inclusions.

In a recent paper [18], we proposed a damage constitutive model of progressive debonding in aligned fiber-reinforced composites. We derived elastic moduli and predicted the overall elastoplastic behavior and damage evolution in aligned fiber-reinforced composites. Using our previous research [18], micromechanical damage constitutive models for two- and three-dimensional (2D and 3D) random fiber reinforced composites are developed in this paper to predict progressive damage in random fiber-reinforced composites. The present micromechanical constitutive model will establish the theoretical foundation needed for simulation of progressive crushing of composite structures. The governing field Equations and overall yield function for aligned-fiber orientations are averaged over all orientations to obtain the constitutive relations and overall yield function of 2D and 3D random fiber-reinforced composites.

In our derivation, fibers are assumed to be elastic spheroids that are embedded in a ductile polymer matrix. Furthermore, the ductile matrix behaves elastoplastically under arbitrary 3D loading/unloading histories. All fibers are assumed to be non-interacting for dilute composite medium and initially embedded firmly in the matrix with perfect interfaces. After the interfacial debonding between fibers and the matrix, these partially debonded fibers are regarded as equivalent, transversely isotropic inclusions. The probability of partial debonding is modeled as a two-parameter, Weibull process. We employ the average internal stresses of fibers as the controlling factor. Small strains are assumed; therefore, the statistical microstructure of fibers embedded in a ductile matrix remains the same. Finally, the present damage models are implemented numerically and compared with experimental data to show the progressive damage behavior of random fiber-reinforced composites.

2. Overall elastoplastic behavior of composites

2.1. Recapitulation of the overall elastoplastic behavior of aligned fiber-reinforced composites

First, an initially perfectly bonded, two-phase composite consisting of a matrix (phase 0) with bulk modulus κ_0 and shear modulus μ_0, and aligned discontinuous, randomly dispersed, spheroidal (prolate) fibers (phase 1) with bulk modulus κ_1 and shear modulus μ_1 is considered. When spheroidal inclusions (discontinuous fibers) are aligned, the composite as a whole is transversely isotropic. Subsequently, as loadings or deformations are applied, some fibers are partially debonded (phase 2). These partially debonded fibers are regarded as equivalent, transversely isotropic inclusions. Following Zhao and Weng [13] and Ju and Lee [17], a partially debonded fiber can be replaced by an equivalent, perfectly bonded fiber that possesses yet unknown transversely isotropic moduli. The transverse isotropy of the equivalent fiber can be determined in such a way that: (a) its tensile and shear stresses will always vanish in the debonded direction; and (b) its stresses in the bonded directions exist because the fiber is still able to transmit stresses to the matrix on the bonded surfaces (see figure 3.1 in Lee [19]).

With the help of Eshelby's tensor for an ellipsoidal inclusion, the effective elastic stiffness tensor $\mathbf{C}_*$ of aligned (in the x_1-direction) fiber-reinforced composites was explicitly derived in our previous research [18] as

$$\mathbf{C}_* = \tilde{F}_{ijkl}(\iota_1, \iota_2, \iota_3, \iota_4, \iota_5, \iota_6) \tag{1}$$

where a transversely isotropic fourth-rank tensor $\tilde{\mathbf{F}}$ is defined by six parameters b_m ($m = 1$–6):

$$\begin{aligned}\tilde{F}_{ijkl}(b_m) = {} & b_1\tilde{n}_i\tilde{n}_j\tilde{n}_k\tilde{n}_l + b_2(\delta_{ik}\tilde{n}_j\tilde{n}_l + \delta_{il}\tilde{n}_j\tilde{n}_k + \delta_{jk}\tilde{n}_i\tilde{n}_l \\ & + \delta_{jl}\tilde{n}_i\tilde{n}_k) + b_3\delta_{ij}\tilde{n}_k\tilde{n}_l + b_4\delta_{kl}\tilde{n}_i\tilde{n}_j + b_5\delta_{ij}\delta_{kl} \\ & + b_6(\delta_{ik}\delta_{jl} + \delta_{il}\delta_{jk})\end{aligned} \tag{2}$$

Here, $\tilde{\mathbf{n}}$ denotes the unit vector and δ_{ij} signifies the Kronecker delta. For a spheroid of $a_1 \neq a_2 = a_3$, in which a_i ($i = 1, 2, 3$) is one of the three semi-axes of the ellipsoid, the 1-direction is chosen as symmetric; therefore, we have $\tilde{n}_1 = 1, \tilde{n}_2 = \tilde{n}_3 = 0$. In addition, the parameters of $\iota_1, \ldots, \iota_6$ in Eq. (1) are

$$\begin{aligned}&\iota_1 = \psi_{11} - \psi_{12} - \psi_{21} + \psi_{22} + 2\varphi_1 + 2\varphi_2 - 4\varphi_3 \\ &\iota_2 = -\varphi_2 + \varphi_3 \qquad \iota_3 = \psi_{21} - \psi_{22} \qquad \iota_4 = \psi_{12} - \psi_{22} \\ &\iota_5 = \psi_{22} \qquad \iota_6 = \varphi_2\end{aligned} \tag{3}$$

in which the parameters $\psi_{11}, \ldots, \psi_{22}$ and $\varphi_1, \ldots, \varphi_3$ are given in the appendix of our previous research [18].

Next, we consider the overall elastoplastic responses of progressively debonded, aligned fiber composites, which initially feature perfect interfacial bonding between fibers

and the matrix in two-phase composites. It is known that partial interfacial debonding may occur in some fibers under applied loading. Therefore, an original two-phase composite may gradually become a three-phase composite consisting of the matrix, perfectly bonded fibers, and partially debonded fibers. We will regard partially debonded fibers as equivalent, perfectly bonded transversely isotropic fibers. For simplicity, the von Mises yield criterion with isotropic hardening law is assumed here. Extension of the present framework to general yield criterion and general hardening law is possible.

An effective yield criterion is derived based on the ensemble-volume averaging process and first-order effects of eigen-strains due to the existence of spheroidal (prolate) fibers. The effective yield criterion, together with the overall associative plastic flow rule and hardening law, establishes the analytical foundation for the estimation of effective elastoplastic behavior of ductile matrix composites. By collecting and summing up all the current stress norm perturbations produced by any typical perfectly bonded fiber and any typical partially debonded fiber and averaging over all possible locations, the ensemble-averaged square of the current stress norm at any matrix point can be derived as

$$\langle H\rangle_m(\mathbf{x}) = \boldsymbol{\sigma}^{\mathrm{o}} : \mathbf{T} : \boldsymbol{\sigma}^{\mathrm{o}} \tag{4}$$

where $\boldsymbol{\sigma}^{\mathrm{o}}$ is the far-field stress and the components of the positive definite fourth-rank tensor $\mathbf{T}$ read

$$T_{ijkl} = \tilde{F}_{ijkl}(\bar{t}_1, \bar{t}_2, \bar{t}_3, \bar{t}_4, \bar{t}_5, \bar{t}_6) \tag{5}$$

in which

$$\bar{t}_1 = \mathscr{M}_{11} - \mathscr{M}_{12} - \mathscr{M}_{21} + \mathscr{M}_{22} + 2\mathscr{N}_1 + 2\mathscr{N}_2 - 4\mathscr{N}_3$$

$$\bar{t}_2 = -\mathscr{N}_2 + \mathscr{N}_3 \qquad \bar{t}_3 = \mathscr{M}_{21} - \mathscr{M}_{23}$$

$$\bar{t}_4 = \mathscr{M}_{12} - \mathscr{M}_{23} \qquad \bar{t}_5 = \mathscr{M}_{23} \qquad \bar{t}_6 = \mathscr{N}_2 \tag{6}$$

here the parameters $\mathscr{M}_{11}, \ldots, \mathscr{M}_{23}$ and $\mathscr{N}_1, \ldots, \mathscr{N}_3$ are given in our previous research [18].

The ensemble-averaged current stress norm at a matrix point can also be expressed in terms of the macroscopic stress $\bar{\boldsymbol{\sigma}}$. Following Ju and Chen [20], the relation between the far-field stress $\boldsymbol{\sigma}^{\mathrm{o}}$ and the macroscopic stress $\bar{\boldsymbol{\sigma}}$ takes the form

$$\boldsymbol{\sigma}^{\mathrm{o}} = \mathbf{P} : \bar{\boldsymbol{\sigma}} \tag{7}$$

where the fourth-rank tensor $\mathbf{P}$ reads

$$\mathbf{P} = [\mathbf{I} + \sum_{r=1}^{2} \phi_r(\mathbf{I} - \mathbf{S})\cdot(\mathbf{A}_r + \mathbf{S})^{-1}]^{-1}$$
$$= \tilde{F}_{ijkl}(p_1, p_2, p_3, p_4, p_5, p_6) \tag{8}$$

in which $\mathbf{I}$ is the fourth-rank identity tensor, ϕ_r denotes the volume fraction of the r-phase, "·" signifies the tensor multiplication, and the fourth-rank tensor $\mathbf{A}_r$ is defined as

$$\mathbf{A}_r \equiv [\mathbf{C}_r - \mathbf{C}_0]^{-1}\cdot\mathbf{C}_0 \tag{9}$$

Here $\mathbf{C}_r$ is the elasticity tensor of the r-phase. The components of Eshelby's tensor $\mathbf{S}$ for a spheroidal inclusion embedded in an isotropic linear elastic and infinite matrix are

$$S_1 = \frac{1}{16}\frac{16 + 45\varpi + 54\alpha^2 + 60\varpi\alpha^2}{(\nu_0 - 1)(1 - \alpha^2)} \qquad S_2 = \frac{1}{16}\frac{8 + 15\varpi - 8\nu_0 - 12\varpi\nu_0 + 2\alpha^2 + 8\nu_0\alpha^2 + 12\varpi\nu_0\alpha^2}{1 - \nu_0 - \alpha^2 + \nu_0\alpha^2}$$

$$S_3 = \frac{1}{16}\frac{3\varpi + 10\alpha^2 + 12\varpi\alpha^2}{(\nu_0 - 1)(\alpha^2 - 1)} \qquad S_4 = \frac{1}{16}\frac{3\varpi + 16\nu_0 + 24\varpi\nu_0 + 10\alpha^2 + 12\varpi\alpha^2 - 16\nu_0\alpha^2 - 24\nu_0\varpi\alpha^2}{(\nu_0 - 1)(\alpha^2 - 1)} \tag{10}$$

$$S_5 = \frac{1}{16}\frac{\varpi - 8\varpi\nu_0 - 2\alpha^2 - 4\varpi\alpha^2 + 8\nu_0\varpi\alpha^2}{(\nu_1 - 1)(\alpha^2 - 1)} \qquad S_6 = \frac{1}{16}\frac{-7\varpi + 8\nu_0\varpi - 2\alpha^2 + 4\varpi\alpha^2 - 8\nu_0\varpi\alpha^2}{1 - \nu_0 - \alpha^2 + \nu_0\alpha^2}$$

with

$$\varpi = \begin{cases} \dfrac{\alpha}{(\alpha^2 - 1)^{3/2}}[\cosh^{-1}\alpha - \alpha(\alpha^2 - 1)^{1/2}], & \text{for } \alpha > 1 \\ \dfrac{\alpha}{(1 - \alpha^2)^{3/2}}[\alpha(1 - \alpha^2)^{1/2} - \cos^{-1}\alpha], & \text{for } \alpha < 1 \end{cases} \tag{11}$$

Here, the spheroid aspect ratio is defined as $\alpha \equiv a_1/a_2$. In addition, the components $p_1, \ldots, p_6$ in Eq. (8) are

$$p_1 = \mathscr{H}_{11} - \mathscr{H}_{12} - \mathscr{H}_{21} + \mathscr{H}_{22} + 2\mathscr{I}_1 + 2\mathscr{I}_2 - 4\mathscr{I}_3$$

$$p_2 = -\mathscr{I}_2 + \mathscr{I}_3 \qquad p_3 = \mathscr{H}_{21} - \mathscr{H}_{23}$$

$$p_4 = \mathscr{H}_{12} - \mathscr{H}_{23} \qquad p_5 = \mathscr{H}_{23} \qquad p_6 = \mathscr{I}_2 \tag{12}$$

where the parameters $\mathscr{H}_{11}, \ldots, \mathscr{H}_{23}$ and $\mathscr{I}_1, \ldots, \mathscr{I}_3$ are given in our previous research [18].

By combining Eqs. (4) and (7), we arrive at the alternative expression for the ensemble-averaged current stress norm (square) at a matrix point

$$\langle H\rangle_m(\mathbf{x}) = \bar{\boldsymbol{\sigma}} : \bar{\mathbf{T}} : \bar{\boldsymbol{\sigma}} \tag{13}$$

where the positive definite fourth-rank tensor $\bar{\mathbf{T}}$ is defined as

$$\bar{\mathbf{T}} = \tilde{F}_{ijkl}(\bar{T}_1, \bar{T}_2, \bar{T}_3, \bar{T}_4, \bar{T}_5, \bar{T}_6) \tag{14}$$

and the parameters $\bar{T}_1, \ldots, \bar{T}_6$ are given in our previous research [18]. More details of elastoplasic stress–strain

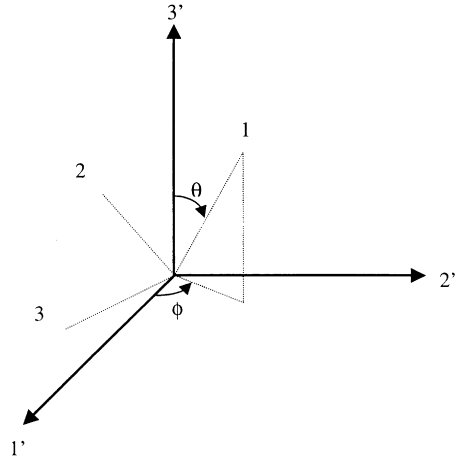

Fig. 1. Spherical coordinates.

relationship for partially debonded, three-phase aligned fiber-reinforced composites can be found in our previous research [18].

2.2. Effective elastic moduli and elastoplastic behavior of randomly oriented fiber-reinforced composites

Consider composite models in which spheroidal fibers with an aspect ratio of α (the ratio of length to diameter) are uniformly dispersed and randomly oriented in 2D or 3D space. The constitutive relations and the overall yield function for randomly oriented composites can be obtained by performing the averaging process over all orientations of governing constitutive field Equations. Accordingly, the constitutive relations and overall yield function for aligned fiber orientations given in Section 2.1 are averaged over all orientations to obtain the constitutive relations and overall yield function of 2D and 3D, randomly oriented fiber-reinforced composites. The overall plastic flow rule and hardening law, with the proposed overall yield function, then characterize the macroscopic elastoplastic behavior of the randomly oriented fiber-reinforced composites under 3D arbitrary loading/unloading histories.

2.2.1. Three-dimensional random fiber orientation

To predict the behavior of a system with a 3D random fiber orientation, it is convenient to introduce a spherical coordinate designation for the direction cosines. Fig. 1 shows the coordinate convention. The local axes of an inclusion are denoted by the unprimed coordinate system and the fixed or material axes by the primed one. Axis 1 is fiber direction and Axis 3 can be taken to lie in the $1'2'$ plane with no loss in generality. Denoting l_{ij} as the direction cosine between the ith primed and jth unprimed axes, we have

$$x'_i = [l_{ij}]x_j \tag{15}$$

where the transformation matrix $[l_{ij}]$ has the form of

$$[l_{ij}] = \begin{bmatrix} \sin\theta\cos\phi & \sin\theta\sin\phi & \cos\theta \\ -\cos\theta\cos\phi & -\cos\theta\sin\phi & \sin\theta \\ \sin\phi & -\cos\phi & 0 \end{bmatrix} \tag{16}$$

Any second-rank tensor (e.g. stress tensor) can be transformed as

$$\sigma'_{ij} = l_{ik}l_{jl}\sigma_{kl} \tag{17}$$

When all inclusions are randomly oriented in the 3D space, the composite as a whole is macroscopically isotropic. The symbol $\subset\cdot\supset$ is used to define the orientational averaging process for all possible orientations as

$$\subset\cdot\supset \equiv \int_0^\pi \int_0^\pi (\cdot)P(\theta,\phi)\sin\theta\,\mathrm{d}\theta\,\mathrm{d}\phi \tag{18}$$

where $P(\theta,\phi)$ is the probability density function. In the special case of uniformly random orientation, we have $P(\theta,\phi) = 1/2\pi$.

For any transversely isotropic fourth-rank tensor $\mathbf{M}$, which takes form of

$$M_{ijkl} = \tilde{F}_{ijkl}(M_1, M_2, M_3, M_4, M_5, M_6) \tag{19}$$

where the transversely isotropic fourth-rank tensor $\tilde{\mathbf{F}}$ is defined in Eq. (2), the following formulation is obtained:

$$\begin{aligned} \subset M_{ijkl} \supset &= \frac{1}{2\pi}\int_0^\pi \int_0^\pi l_{mi}l_{nj}M_{mnpq}l_{pk}l_{ql}\sin\theta\,\mathrm{d}\theta\,\mathrm{d}\phi \\ &= \zeta_1\delta_{ij}\delta_{kl} + \zeta_2(\delta_{ik}\delta_{jl} + \delta_{il}\delta_{jk}) \end{aligned} \tag{20}$$

in which

$$\zeta_1 = \frac{1}{15}[M_1 + 5(M_3 + M_4 + 3M_5)] \tag{21}$$

$$\zeta_2 = \frac{1}{15}[M_1 + 10M_2 + 15M_6] \tag{22}$$

The formulation in Eq. (20) shows that, after the 3D orientational averaging process, any transversely isotropic fourth-rank tensor will become an isotropic fourth-rank tensor.

Assuming the uniform distribution of overall strains [21], with the help of the formulation in Eq. (20), the effective elasticity tensor $\subset \mathbf{C}_* \supset$ of 3D random fiber composites can be obtained as

$$\subset \mathbf{C}_* \supset = \tilde{c}_1\delta_{ij}\delta_{kl} + \tilde{c}_2(\delta_{ik}\delta_{jl} + \delta_{il}\delta_{jk}) \tag{23}$$

where

$$\tilde{c}_1 = \frac{1}{15}[\iota_1 + 5(\iota_3 + \iota_4 + 3\iota_5)] \tag{24}$$

$$\tilde{c}_2 = \frac{1}{15}[\iota_1 + 10\iota_2 + 15\iota_6] \tag{25}$$

Here the parameters of $\iota_1, \ldots, \iota_6$ are given in Eq. (3). Moreover, the effective Young's modulus E_* and Poisson's ratio

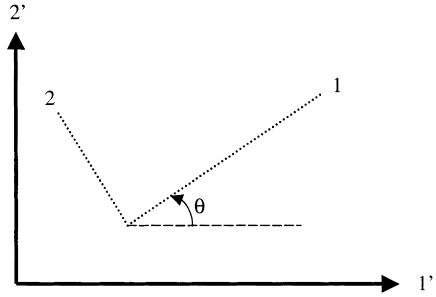

Fig. 2. Planar coordinates.

ν_* of 3D random fiber composites are easily obtained through the following relations

$$E_* = \frac{\tilde{c}_2(3\tilde{c}_1 + 2\tilde{c}_2)}{\tilde{c}_1 + \tilde{c}_2} \tag{26}$$

$$\nu_* = \frac{\tilde{c}_1}{2(\tilde{c}_1 + \tilde{c}_2)} \tag{27}$$

We now consider the overall elastoplastic responses of progressively debonded composites with randomly oriented fibers in 3D space. By using the orientational averaging process in Eq. (20), the orientation-averaged square of stress norm $\subset H_m \supset$ at any matrix point can be obtained as

$$\subset H_m \supset = \boldsymbol{\sigma}^{\mathrm{o}} : \subset \mathbf{T} \supset : \boldsymbol{\sigma}^{\mathrm{o}} \tag{28}$$

where the isotropic fourth-rank tensor $\subset \mathbf{T} \supset$ is

$$\subset T_{ijkl} \supset = \frac{1}{2\pi} \int_0^{\pi} \int_0^{\pi} l_{mi} l_{nj} T_{mnpq} l_{pk} l_{ql} \sin\theta \, \mathrm{d}\theta \, \mathrm{d}\phi \tag{29}$$

The components of the positive definite fourth-rank tensor $\subset \mathbf{T} \supset$ read

$$\subset T_{ijkl} \supset = \tilde{t}_1 \delta_{ij}\delta_{kl} + \tilde{t}_2(\delta_{ik}\delta_{jl} + \delta_{il}\delta_{jk}) \tag{30}$$

with

$$\tilde{t}_1 = \frac{1}{15}[\bar{t}_1 + 5(\bar{t}_3 + \bar{t}_4 + 3\bar{t}_5)] \tag{31}$$

$$\tilde{t}_2 = \frac{1}{15}[\bar{t}_1 + 10\bar{t}_2 + 15\bar{t}_6] \tag{32}$$

where the parameters $\bar{t}_1, \ldots, \bar{t}_6$ are given in Eq. (6).

In Eq. (28), $\subset H_m \supset$ is described in terms of the far-field stress $\boldsymbol{\sigma}^{\mathrm{o}}$. Alternatively, the orientation-averaged square of the stress norm can also be expressed in terms of the macroscopic (orientation-averaged) stress $\subset \bar{\boldsymbol{\sigma}} \supset$. Following our previous research [18], the relationship between the far-field stress $\boldsymbol{\sigma}^{\mathrm{o}}$ and the macroscopic stress $\subset \bar{\boldsymbol{\sigma}} \supset$ takes the form

$$\boldsymbol{\sigma}^{\mathrm{o}} = \subset \mathbf{P} \supset : \subset \bar{\boldsymbol{\sigma}} \supset \tag{33}$$

where the fourth-rank tensor $\subset \mathbf{P} \supset$ reads

$$\subset P_{ijkl} \supset = \left[I_{ijkl} + \sum_{r=1}^{2} \frac{\phi_r}{2\pi} \int_0^{\pi} \int_0^{\pi} Q_{mi} Q_{nj} [I_{mnpq} - S_{mnpq}] \times [(A_r)_{pqst} + S_{pqst}]^{-1} Q_{sk} Q_{tl} \sin\theta \, \mathrm{d}\theta \, \mathrm{d}\phi \right]^{-1}$$

$$= \tilde{p}_1 \delta_{ij}\delta_{kl} + \tilde{p}_2(\delta_{ik}\delta_{jl} + \delta_{il}\delta_{jk}) \tag{34}$$

with

$$\tilde{p}_1 = \tfrac{1}{15}[p_1 + 5(p_3 + p_4 + 3p_5)] \tag{35}$$

$$\tilde{p}_2 = \tfrac{1}{15}[p_1 + 10p_2 + 15p_6] \tag{36}$$

where the parameters $p_1, \ldots, p_6$ are given in Eq. (12).

By combining Eqs. (28) and (33), we arrive at the alternative expression for the orientation-averaged current stress norm (square) at a matrix point:

$$\subset H_m \supset = \subset \bar{\boldsymbol{\sigma}} \supset : \subset \bar{\mathbf{T}} \supset : \subset \bar{\boldsymbol{\sigma}} \supset \tag{37}$$

where

$$\subset \bar{\mathbf{T}} \supset = \subset \mathbf{P} \supset^{\mathrm{T}} \cdot \subset \mathbf{T} \supset \cdot \subset \mathbf{P} \supset$$

$$= \bar{T}_1 \delta_{ij}\delta_{kl} + \bar{T}_2(\delta_{ik}\delta_{jl} + \delta_{il}\delta_{jk}) \tag{38}$$

with

$$\bar{T}_1 = [3\tilde{p}_1 + 2\tilde{p}_2]^2 \tilde{t}_1 + 2\tilde{p}_1\tilde{t}_2[3\tilde{p}_1 + 4\tilde{p}_2] \tag{39}$$

$$\tilde{T}_2 = 4[\tilde{p}_2]^2 \tilde{t}_2. \tag{40}$$

2.2.2. Two-dimensional, planar random fiber orientation

When the spheroidal inclusions are randomly oriented in the 1-2 plane, the composite is transversely isotropic. Such a system exists in sheet molding compounds (SMC). The derivation of effective properties for 2D, plane stress, random fiber orientation proceeds in the same manner as in the 3D case. Fig. 2 shows planar coordinates. The local axes of an inclusion are denoted by the unprimed coordinate system and the fixed or material axes by the primed one. Axis 1 is fiber direction. When the randomness exists only in the 1-2 plane, resulting in a planar (transversely isotropic) composite, the transformation matrix $[l_{ij}]$ becomes

$$[l_{ij}] = \begin{bmatrix} \cos\theta & \sin\theta & 0 \\ -\sin\theta & \cos\theta & 0 \\ 0 & 0 & 1 \end{bmatrix}. \tag{41}$$

Similarly, the orientational averaging process, denoted by $\langle\langle\cdot\rangle\rangle$, for the planar random orientation can be defined as

$$\langle\langle\cdot\rangle\rangle \equiv \int_0^{\pi} (\cdot) P(\theta) \, \mathrm{d}\theta \tag{42}$$

where $P(\theta)$ is the probability density function. In the special case of uniformly random orientation, we have $P(\theta) = 1/\pi$.

For any transversely isotropic fourth-rank tensor **M** defined in Eq. (19), the following formulation is obtained

$$\langle\langle M_{ijkl}\rangle\rangle = \frac{1}{\pi}\int_0^{\pi} Q_{mi}Q_{nj}M_{mnpq}Q_{pk}Q_{ql}\sin\theta\,\mathrm{d}\theta = \tilde{F}_{ijkl}(\varpi_1,\varpi_2,\varpi_3,\varpi_4,\varpi_5,\varpi_6) \tag{43}$$

where

$$\begin{aligned}
&\varpi_1 = \tfrac{3}{8}M_1 \qquad \varpi_2 = -\tfrac{1}{8}[M_1 + 4M_2]\\
&\varpi_3 = -\tfrac{1}{8}[M_1 + 4M_3] \qquad \varpi_4 = -\tfrac{1}{8}[M_1 + 4M_4]\\
&\varpi_5 = \tfrac{1}{8}[M_1 + 4(M_3 + M_4 + 2M_5)]\\
&\varpi_6 = \tfrac{1}{8}M_1 + M_2 + M_6
\end{aligned} \tag{44}$$

The formulation in Eq. (43) shows that, after the 2D orientational averaging process, any transversely isotropic fourth-rank tensor will remain so.

Assuming the uniform distribution of overall strains, with the help of the formulation in Eq. (43), the effective elasticity tensor $\subset \mathbf{C}_* \supset$ of 2D random fiber composites can be obtained as

$$\langle\langle \mathbf{C}_*\rangle\rangle = \tilde{F}_{ijkl}(\hat{c}_1,\hat{c}_2,\hat{c}_3,\hat{c}_4,\hat{c}_5,\hat{c}_6) \tag{45}$$

where

$$\begin{aligned}
&\hat{c}_1 = \tfrac{3}{8}\iota_1 \qquad \hat{c}_2 = -\tfrac{1}{8}[\iota_1 + 4\iota_2] \qquad \hat{c}_3 = -\tfrac{1}{8}[\iota_1 + 4\iota_3]\\
&\hat{c}_4 = -\tfrac{1}{8}[\iota_1 + 4\iota_4] \qquad \hat{c}_5 = \tfrac{1}{8}[\iota_1 + 4(\iota_3 + \iota_4 + 2\iota_5)]\\
&\hat{c}_6 = \tfrac{1}{8}\iota_1 + \iota_2 + \iota_6
\end{aligned} \tag{46}$$

The parameters of $\iota_1,\ldots,\iota_6$ are given in Eq. (3). In addition, Young's moduli E_{L}, E_{T}; shear moduli μ_{L}, μ_{T}; and Poisson's ratios ν_{LT}, ν_{TT}, ν_{TT} of the transversely isotropic composites can be obtained as

$$E_{\mathrm{L}} = \hat{c}_1 + 4\hat{c}_2 + \hat{c}_3 + \hat{c}_4 + \hat{c}_5 + 2\hat{c}_6 - \frac{(\hat{c}_3 + \hat{c}_5)^2}{\hat{c}_5 + \hat{c}_6} \tag{47}$$

$$E_{\mathrm{T}} = \frac{4\hat{c}_6[(\hat{c}_1 + 4\hat{c}_2 + \hat{c}_3 + \hat{c}_4 + \hat{c}_5 + 2\hat{c}_6)(\hat{c}_5 + \hat{c}_6) - (\hat{c}_3 + \hat{c}_5)^2]}{(\hat{c}_1 + 4\hat{c}_2 + \hat{c}_3 + \hat{c}_4 + \hat{c}_5 + 2\hat{c}_6)(\hat{c}_5 + 2\hat{c}_6) - (\hat{c}_3 + \hat{c}_5)^2} \tag{48}$$

$$\mu_{\mathrm{L}} = \hat{c}_2 + \hat{c}_6 \tag{49}$$

$$\mu_{\mathrm{T}} = \hat{c}_6 \tag{50}$$

$$\nu_{\mathrm{LT}} = \frac{\hat{c}_3 + \hat{c}_5}{2(\hat{c}_2 + \hat{c}_5 + \hat{c}_6)} \tag{51}$$

$$\nu_{\mathrm{TL}} = \frac{2\hat{c}_6(\hat{c}_3 + \hat{c}_5)}{(\hat{c}_1 + 4\hat{c}_2 + \hat{c}_3 + \hat{c}_4 + \hat{c}_5 + 2\hat{c}_6)(\hat{c}_5 + 2\hat{c}_6) - (\hat{c}_3 + \hat{c}_5)^2} \tag{52}$$

$$\nu_{\mathrm{TT}} = \frac{\hat{c}_5(\hat{c}_1 + 4\hat{c}_2 + \hat{c}_3 + \hat{c}_4 + \hat{c}_5 + 2\hat{c}_6) - (\hat{c}_3 + \hat{c}_5)^2}{(\hat{c}_1 + 4\hat{c}_2 + \hat{c}_3 + \hat{c}_4 + \hat{c}_5 + 2\hat{c}_6)(\hat{c}_5 + 2\hat{c}_6) - (\hat{c}_3 + \hat{c}_5)^2} \tag{53}$$

where the subscripts L and T represent properties along and at right angles to the fibers.

We now consider the overall elastoplastic responses of progressively debonded composites with randomly oriented fibers in the 2D space. By using the orientational averaging process in Eq. (43), the orientation-averaged square of stress norm $\langle\langle H_m\rangle\rangle$ at any matrix point can be obtained as

$$\langle\langle H_m\rangle\rangle = \boldsymbol{\sigma}^{\mathrm{o}} : \langle\langle \mathbf{T}\rangle\rangle : \boldsymbol{\sigma}^{\mathrm{o}} \tag{54}$$

where the transversely isotropic fourth-rank tensor $\langle\langle \mathbf{T}\rangle\rangle$ is

$$\langle\langle T_{ijkl}\rangle\rangle = \frac{1}{\pi}\int_0^{\pi} l_{mi}l_{nj}T_{mnpq}l_{pk}l_{ql}\,\mathrm{d}\theta \tag{55}$$

The components of the positive definite fourth-rank tensor $\langle\langle \mathbf{T}\rangle\rangle$ read

$$\langle\langle T_{ijkl}\rangle\rangle = \tilde{F}_{ijkl}(\hat{t}_1,\hat{t}_2,\hat{t}_3,\hat{t}_4,\hat{t}_5,\hat{t}_6) \tag{56}$$

with

$$\begin{aligned}
&\hat{t}_1 = \tfrac{3}{8}\bar{t}_1 \qquad \hat{t}_2 = -\tfrac{1}{8}[\bar{t}_1 + 4\bar{t}_2] \qquad \hat{t}_3 = -\tfrac{1}{8}[\bar{t}_1 + 4\bar{t}_3]\\
&\hat{t}_4 = -\tfrac{1}{8}[\bar{t}_1 + 4\bar{t}_4] \qquad \hat{t}_5 = \tfrac{1}{8}[\bar{t}_1 + 4(\bar{t}_3 + \bar{t}_4 + 2\bar{t}_5)]\\
&\hat{t}_6 = \tfrac{1}{8}\bar{t}_1 + \bar{t}_2 + \bar{t}_6
\end{aligned} \tag{57}$$

where the parameters $\bar{t}_1,\ldots,\bar{t}_6$ are given in Eq. (6).

Similarly, the relationship between the far-field stress $\boldsymbol{\sigma}^{\mathrm{o}}$ and the macroscopic (orientation-averaged) stress $\langle\langle\bar{\sigma}\rangle\rangle$ takes the form

$$\boldsymbol{\sigma}^{\mathrm{o}} = \langle\langle \mathbf{P}\rangle\rangle : \langle\langle\bar{\boldsymbol{\sigma}}\rangle\rangle \tag{58}$$

where the fourth-rank tensor $\langle\langle \mathbf{P}\rangle\rangle$ reads

$$\langle\langle P\rangle\rangle_{ijkl} = \left[I_{ijkl} + \sum_{r=1}^{2}\frac{\phi_r}{\pi}\int_0^{\pi} Q_{mi}Q_{nj}[I_{mnpq} - S_{mnpq}]\cdot[(A_r)_{pqst} + S_{pqst} + S_{pqst}]^{-1}Q_{sk}Q_{tl}\,\mathrm{d}\theta\right]^{-1} = \tilde{F}_{ijkl}(\hat{p}_1,\hat{p}_2,\hat{p}_3,\hat{p}_4,\hat{p}_5,\hat{p}_6) \tag{59}$$

with

$$\hat{p}_1 = \tfrac{3}{8}p_1 \tag{60}$$

$$\hat{p}_2 = -\tfrac{1}{8}[p_1 + 4p_2] \tag{61}$$

$$\hat{p}_3 = -\tfrac{1}{8}[p_1 + 4p_3] \tag{62}$$

$$\hat{p}_4 = -\tfrac{1}{8}[p_1 + 4p_4] \tag{63}$$

$$\hat{p}_5 = \tfrac{1}{8}[p_1 + 4(p_3 + p_4 + 2p_5)] \tag{64}$$

$$\hat{p}_6 = \tfrac{1}{8}p_1 + p_2 + p_6 \tag{65}$$

where the parameters $p_1, \ldots, p_6$ are given in Eq. (12).

By combining Eqs. (54) and (58), we arrive at the alternative expression for the orientation-averaged current stress norm (square) at a matrix point

$$\langle\langle H_m \rangle\rangle = \langle\langle \bar{\sigma} \rangle\rangle : \langle\langle \bar{\mathbf{T}} \rangle\rangle : \langle\langle \bar{\boldsymbol{\sigma}} \rangle\rangle \tag{66}$$

where

$$\langle\langle \bar{\mathbf{T}} \rangle\rangle = \langle\langle \mathbf{P} \rangle\rangle^{\mathbf{T}} \cdot \langle\langle \mathbf{T} \rangle\rangle : \langle\langle \mathbf{P} \rangle\rangle = \tilde{F}_{ijkl}(\hat{T}_1, \hat{T}_2, \hat{T}_3, \hat{T}_4, \hat{T}_5, \hat{T}_6) \tag{67}$$

with

$$\begin{aligned}\hat{T}_1 = {} & 4\hat{p}_1\hat{p}_6\hat{t}_6 + 8(\hat{p}_1 + 2\hat{p}_2 + \hat{p}_3)(\hat{p}_2\hat{t}_2 + \hat{p}_6\hat{t}_2 + \hat{p}_2\hat{t}_6) \\ & + (\hat{p}_1 + 4\hat{p}_2 + 3\hat{p}_3)(\hat{p}_1\hat{t}_4 + 4\hat{p}_2\hat{t}_4 + \hat{p}_4\hat{t}_4 + 2\hat{p}_6\hat{t}_4 \\ & + \hat{p}_1\hat{t}_5 + 4\hat{p}_2\hat{t}_5 + 3\hat{p}_4\hat{t}_5 + 2\hat{p}_4\hat{t}_6) + (\hat{p}_1 + 4\hat{p}_2 + \hat{p}_3 \\ & + 2\hat{p}_6)[2\hat{p}_6\hat{t}_1 + 4\hat{p}_2(\hat{t}_1 + 2\hat{t}_2 + \hat{t}_3) + \hat{p}_4(\hat{t}_1 + 4\hat{t}_2 \\ & + 3\hat{t}_3) + \hat{p}_1(\hat{t}_1 + 4\hat{t}_2 + \hat{t}_3 + 2\hat{t}_6)]\end{aligned} \tag{68}$$

$$\hat{T}_2 = 4(\hat{p}_2\hat{p}_2\hat{t}_2 + 2\hat{p}_2\hat{p}_6\hat{t}_2 + \hat{p}_6\hat{p}_6\hat{t}_2 + \hat{p}_2\hat{p}_2\hat{t}_6 + 2\hat{p}_2\hat{p}_6\hat{t}_6) \tag{69}$$

$$\begin{aligned}\hat{T}_3 = {} & 4\hat{p}_3\hat{p}_6\hat{t}_6 + (\hat{p}_1 + 4\hat{p}_2 + 3\hat{p}_3)(\hat{p}_3\hat{t}_4 + \hat{p}_5\hat{t}_4 + \hat{p}_3\hat{t}_5 + 3\hat{p}_5\hat{t}_5 \\ & + 2\hat{p}_6\hat{t}_5 + 2\hat{p}_5\hat{t}_6) + (\hat{p}_1 + 4\hat{p}_2 + \hat{p}_3 + 2\hat{p}_6)[2\hat{p}_6\hat{t}_3 \\ & + \hat{p}_5(\hat{t}_1 + 4\hat{t}_2 + 3\hat{t}_3) + \hat{p}_3(\hat{t}_1 + 4\hat{t}_2 + \hat{t}_3) + 2\hat{t}_6)]\end{aligned} \tag{70}$$

$$\begin{aligned}\hat{T}_4 = {} & 4\hat{p}_4\hat{p}_6\hat{t}_6 + 8(\hat{p}_4 + \hat{p}_5)(\hat{p}_2\hat{t}_2 + \hat{p}_6\hat{t}_2 + \hat{p}_2\hat{t}_6) + (\hat{p}_4 + 3\hat{p}_5 \\ & + 2\hat{p}_6)(\hat{p}_1\hat{t}_4 + 4\hat{p}_2\hat{t}_4 + \hat{p}_4\hat{t}_4 + 2\hat{p}_6\hat{t}_4 + \hat{p}_1\hat{t}_5 + 4\hat{p}_2\hat{t}_5 \\ & + 3\hat{p}_4\hat{t}_5 + 2\hat{p}_4\hat{t}_6) + (\hat{p}_4 + \hat{p}_5)[2\hat{p}_6\hat{t}_1 + 4\hat{p}_2(\hat{t}_1 + 2\hat{t}_2 \\ & + \hat{t}_3) + \hat{p}_4(\hat{t}_1 + 4\hat{t}_2 + 3\hat{t}_3) + \hat{p}_1(\hat{t}_1 + 4\hat{t}_2 + \hat{t}_3 + 2\hat{t}_6)]\end{aligned} \tag{71}$$

$$\begin{aligned}\hat{T}_5 = {} & 4\hat{p}_5\hat{p}_6\hat{t}_6 + (\hat{p}_4 + 3\hat{p}_5 + 2\hat{p}_6)(\hat{p}_3\hat{t}_4 + \hat{p}_5\hat{t}_4 + \hat{p}_3\hat{t}_5 \\ & + 3\hat{p}_5\hat{t}_5 + 2\hat{p}_6\hat{t}_5 + 2\hat{p}_5\hat{t}_6) + (\hat{p}_4 + \hat{p}_5)[2\hat{p}_6\hat{t}_3 + \hat{p}_5(\hat{t}_1 \\ & + 4\hat{t}_2 + 3\hat{t}_3) + \hat{p}_3(\hat{t}_1 + 4\hat{t}_2 + \hat{t}_3 + 2\hat{t}_6)\end{aligned} \tag{72}$$

$$\hat{T}_6 = 4\hat{p}_6\hat{p}_6\hat{t}_6. \tag{73}$$

2.2.3. Averaged yield function for randomly oriented fiber-reinforced composites

The ensemble-volume averaged "current stress norm" for any point in 3D random fiber composites can be defined as

$$\sqrt{\langle H \rangle(\mathbf{x})} = (1 - \phi_1)\sqrt{\subset \bar{\boldsymbol{\sigma}} \supset : \subset \bar{\mathbf{T}} \supset : \subset \bar{\boldsymbol{\sigma}} \supset} \tag{74}$$

where ϕ_1 is the current volume fraction of perfectly bonded fibers. Therefore, the effective yield function for the three-phase, 3D random fiber composites can be proposed as

$$\bar{F} = (1 - \phi_1)^2 \subset \bar{\boldsymbol{\sigma}} \supset : \subset \bar{\mathbf{T}} \supset : \subset \bar{\boldsymbol{\sigma}} \supset - K^2(\bar{e}^p) \tag{75}$$

with the isotropic hardening function $K(\bar{e}^p)$ for the three-phase composite. The effective ensemble-volume averaged plastic strain rate for the 3D random fiber composites can be expressed as

$$\dot{\bar{\boldsymbol{\epsilon}}}^p = \dot{\lambda}\,\frac{\partial \bar{F}}{\partial \bar{\boldsymbol{\sigma}}} = 2(1 - \phi_1)^2 \dot{\lambda} \subset \bar{\mathbf{T}} \supset : \subset \bar{\boldsymbol{\sigma}} \supset \tag{76}$$

where $\dot{\lambda}$ signifies the plastic consistency parameter.

The effective equivalent plastic strain rate for the composite is defined as

$$\begin{aligned}\dot{\bar{e}}^p &\equiv \sqrt{\tfrac{2}{3}\dot{\bar{\boldsymbol{\epsilon}}}^p : \subset \bar{\mathbf{T}} \supset^{-1} : \dot{\bar{\boldsymbol{\epsilon}}}^p} \\ &= 2(1 - \phi_1)^2 \dot{\lambda}\sqrt{\tfrac{2}{3} \subset \bar{\boldsymbol{\sigma}} \supset : \subset \bar{\mathbf{T}} \supset : \subset \bar{\boldsymbol{\sigma}} \supset}\end{aligned} \tag{77}$$

The $\dot{\lambda}$ together with the yield function $\bar{F}$ must obey the *Kuhn-Tucker* loading/unloading conditions. The simple power-law type isotropic hardening function is employed as an example:

$$K(\bar{e}^p) = \sqrt{\tfrac{2}{3}}\{\sigma_y + h(\bar{e}^p)^{\bar{q}}\} \tag{78}$$

where σ_y is the initial yield stress, and h and $\bar{q}$ signify the linear and exponential isotropic hardening parameters (respectively) for the three-phase composite. For 2D, planar random fiber composites, $\subset \bar{\boldsymbol{\sigma}} \supset$ and $\subset \bar{\mathbf{T}} \supset$ in Eqs. (74)–(77) are replaced by $\langle\langle \bar{\boldsymbol{\sigma}} \rangle\rangle$ and $\langle\langle \bar{\mathbf{T}} \rangle\rangle$, respectively.

3. Progressive fiber debonding

The evolutionary interfacial debonding occurs under increasing loads or deformations and influences the overall behavior of randomly oriented, discontinuous fiber-reinforced composites. After the interfacial debonding, the debonded fibers may lose the load-carrying capacity in the debonded direction and can be regarded as partially debonded fibers. Within the context of the first-order (noninteracting) approximation, the stresses inside fibers should be uniform. For convenience, following Zhao and Weng [13,14] and Ju and Lee [17], the probability of partial debonding is modeled as a two-parameter, Weibull process. We employ the average internal stresses of fibers as the controlling factor. Assuming that the Weibull statistics govern, the cumulative probability distribution function of fiber debonding (damage) P_d at the level of hydrostatic tensile stress can be expressed as

$$P_d[(\bar{\boldsymbol{\sigma}}_m)_1] = 1 - \exp\left[-\left(\frac{(\bar{\boldsymbol{\sigma}}_m)_1}{S_o}\right)^M\right] \tag{79}$$

where $(\bar{\boldsymbol{\sigma}}_m)_1 = [(\bar{\sigma}_{11})_1 + (\bar{\sigma}_{22})_1 + (\bar{\sigma}_{33})_1]/3$ is the hydrostatic tensile stresses of the fibers, the subscript $(\cdot)_1$ denotes the fiber phase, and S_o and M are the Weibull parameters.

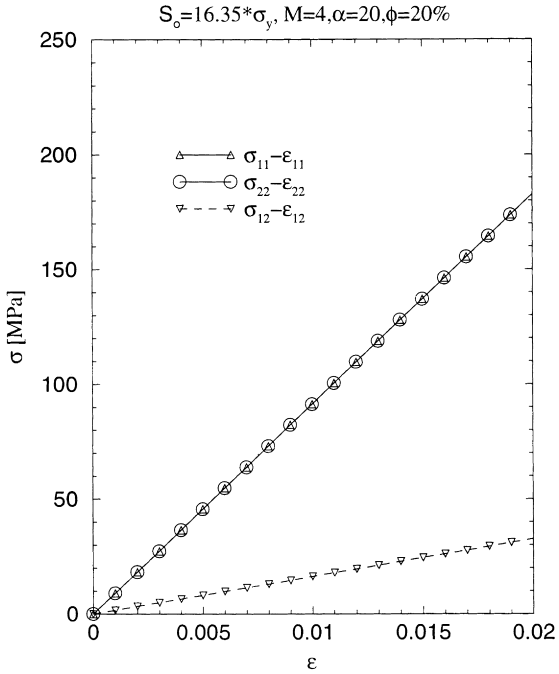

Fig. 3. Stress–strain relations of a two-dimensional random fiber-reinforced composite under uniform deformations.

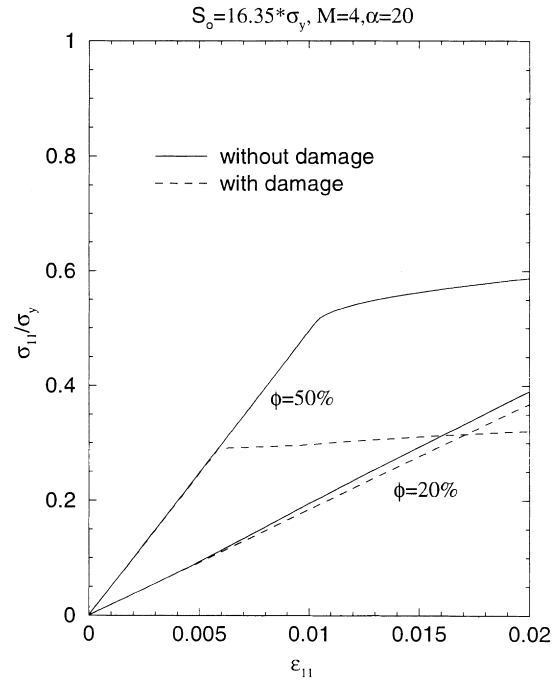

Fig. 4. Effect of the initial volume fraction of fibers on the overall elasto-plastic damage behavior of three-dimensional random fiber-reinforced composites.

Therefore, the current partially debonded (damaged) fiber volume fraction ϕ_2 at a given level of $(\bar{\boldsymbol{\sigma}}_m)_1$ is given by

$$\phi_2 = \phi P_d[(\bar{\boldsymbol{\sigma}}_m)_1] = \phi\left\{1 - \exp\left[-\left(\frac{(\bar{\boldsymbol{\sigma}}_m)_1}{S_o}\right)^M\right]\right\} \qquad (80)$$

where ϕ is the original fiber volume fraction.

The internal stresses of fibers required for the initiation of interfacial debonding can be found in Ju and Lee [17] and our previous research [18].

4. Examples and discussion

In our previous research [18], we compared the present analytical predictions with bounds based on Halpin–Tsai micromechanics equations [22] to validate the proposed micromechanical framework for aligned, discontinuous fiber-reinforced composites. One of the advantages of the Halpin–Tsai equations is that they cover both the particulate reinforced case (fiber aspect ratio = unity, lower bound) and the continuous fiber case (fiber aspect ratio = infinity, upper bound). We plotted the theoretical predictions based on Halpin–Tsai's bounds and the proposed method with various fiber aspect ratios. Clearly, our analytical predictions were well within the Halpin–Tsai's bounds (see Fig. 2 in Lee and Simunovic [18]).

To illustrate the elastoplastic behavior of the present damage constitutive framework, our present damage models for 2D and 3D random fiber composites considering interfacial debonding are presented in Figs. 3–5. The material properties of random fiber composites involving these simulations are $E_0 = 3.0$ GPa, $\nu_0 = 0.35$, $E_1 = 380$ GPa, $\nu_1 = 0.25$, $\alpha = 20$, $\sigma_y = 125$ MPa, $h = 400$ MPa, and $\bar{q} = 0.5$. In addition, to implement the proposed probabilistic micromechanics based on Weibull function into the present constitutive models, we need to estimate the values of

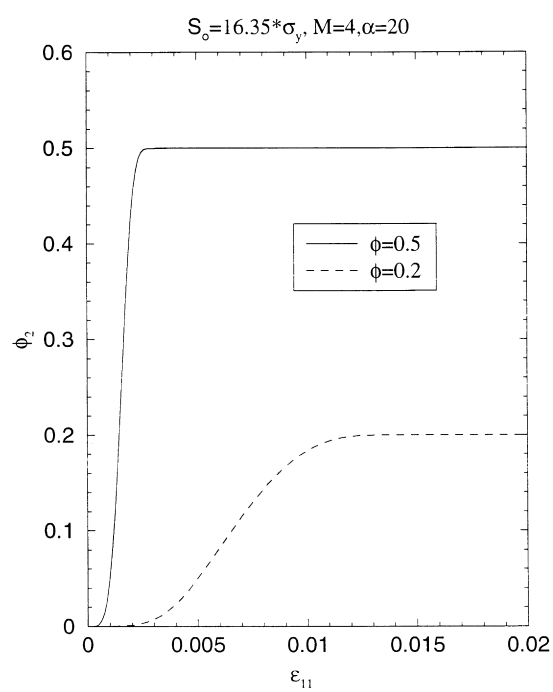

Fig. 5. The predicted evolution of debonded fiber volume fraction corresponding to Fig. 4.

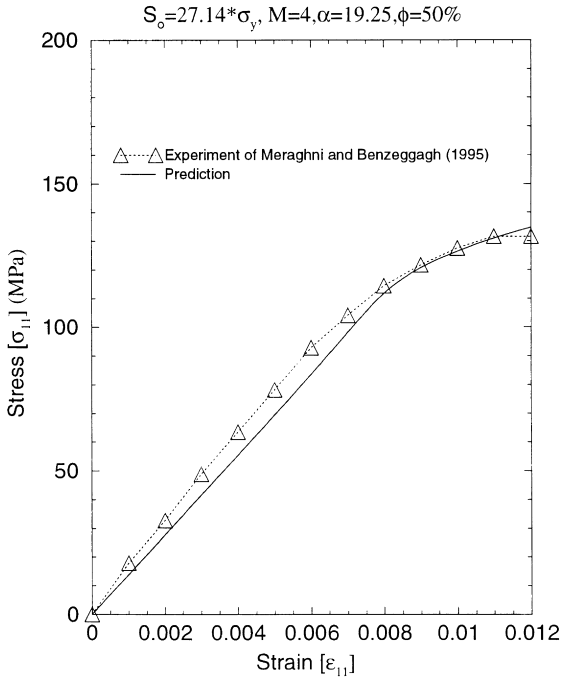

Fig. 6. The prediction between the present prediction and experimental data for overall uniaxial tensile responses of randomly oriented discontinuous fiber composites with initial fiber volume fraction of 0.5.

Weibull partameters S_o and M. For simplicity, we assume the Weibull parameters to be $S_o = 16.35 \times \sigma_y$ and $M = 4$. First, the stress–strain relations of a 2D random fiber-reinforced composite under uniform deformations for the planar random orientation are presented in Fig. 3. It shows a typical

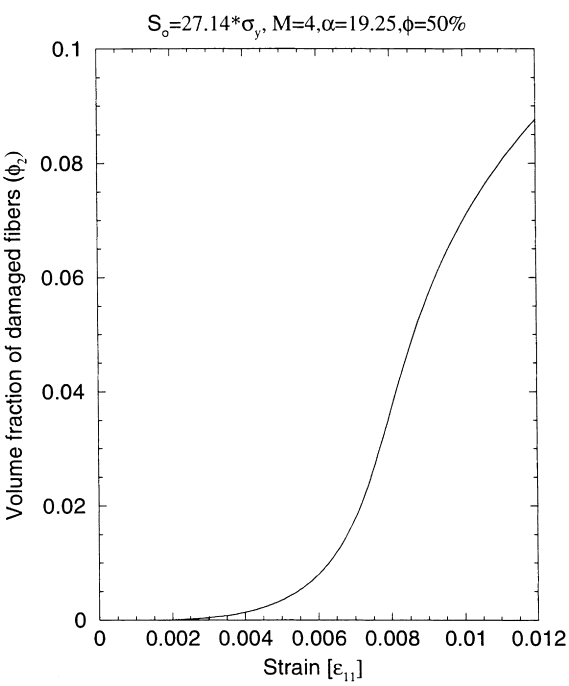

Fig. 7. The predicted evolution of debonded fiber volume fraction versus strain corresponding to Fig. 6.

transversely isotropic behavior as expected. Fig. 4 exhibits the effect of the initial volume fraction of fibers on the behavior and progressive debonding of 3D random fiber composites and includes the results for perfect composites shown by solid lines and debonded composites shown by dashed lines. More interfacial debonding is observed for high-fiber volume fraction ($\phi = 0.5$) composites. Fig. 5 shows the evolutions of debonded fiber volume fraction as a function of the uniaxial strain. It is seen that the composite with high initial volume fraction of fibers is stiffer, but the influence of damage on the stress–strain response of the composite is more drastic because of quick damage evolution.

We further compare our prediction with the experimental data provided by Meraghni and Benzeggagh [10] for 3D random fiber composites. Here, we adopt the elastic properties, aspect ratio, and fiber volume fraction according to Mergahni and Benzeggagh [10] as follows: $E_0 = 3.0$ GPa, $\nu_0 = 0.35$, $E_1 = 72$ GPa, $\nu_1 = 0.17$, $\alpha = 19.25$, and $\phi_1 = 0.5$. Using the parameter estimation algorithm developed by Ju et al. [23] and Simo et al. [24], we estimate the plastic parameters σ_y, h, and $\bar{q}$ in accordance with the isotropic hardening law given in Eq. (78) and Weibull parameters S_o and M for evolutionary debonding to be $\sigma_y = 150$ MPa, $h = 400$ MPa, $\bar{q} = 0.5$, $S_o = 27.14 \times \sigma_y$, and $M = 4.0$. We depict our prediction against the experimental data provided by Meraghni and Benzeggagh [10] in Figs. 6 and 7. Due to the small-strain constraint, we do not display our prediction beyond $\epsilon_{11} = 0.012$. Since our formulation does not consider inter-fiber interaction, the stress–strain curve for the present prediction is lower than that based on the experiment in the early stage. Naturally, the overall stiffness of interacting damage model is higher than that of noninteracting damage model [19]. As the strain increases, the effect of damage becomes the dominant one; therefore, the curves corresponding to the present prediction and the experiment will intersect each other because the proposed damage constitutive model includes the interfacial debonding only. Therefore, it is concluded that the interaction effect among constituents must be considered in modeling damage behavior of composites for both moderately and extremely high fiber volume fraction. Furthermore, other damage mechanisms (e.g. matrix cracking, void nucleation, etc.) must be included in the damage constitutive models to offer more realistic damage predictions.

Finally, the present model does not account for other damage mechanisms because these effects are beyond the scope of the present work. In spite of these limitations, the agreement between the present predictions and experiments is encouraging for possible use of the proposed damage constitutive models for predicting the progressive damage in composite structures. The present micromechanical constitutive model also establishes the theoretical foundation needed for simulation of progressive crushing of composite structures. In a forthcoming paper, implementation of the proposed damage models into finite element program DYNA3D will be presented to show the dynamic

inelastic behavior and progressive crushing in composites under impact loading. Specifically, inter-fiber interactions, microcrack-weakened composites, large-strain formulation, and finite element examples will be addressed.

Acknowledgements

This research was sponsored by the US Department of Energy, Assistant Secretary for Energy Efficiency and Renewable Energy, Office of Transportation Technologies, Lightweight Materials Program, under contract DE-AC05-96OR22464 with Lockheed Martin Energy Research Corporation. The research was supported in part by an appointment to the Oak Ridge National Laboratory Postdoctoral Research Associates Program administered jointly by the Oak Ridge National Laboratory and the Oak Ridge Institute for Science and Education.

References

[1] Ibnabdeljalil M, Phoenix SL. Statistical failure of brittle matrix composites with discontinuous fiber—I. Analysis and Monte Carlo simulation. Acta Metall Mater 1995;43:2975–83.
[2] Wu HC, Li VC. Stochastic process of multiple cracking in discontinuous random fiber reinforced brittle matrix composites. Int J Damage Mech 1995;4:83–102.
[3] Wang M, Laird C. Characterization of microstructure and tensile behavior of a cross-woven C–SiC composites. Acta Mater 1996;44:1371–87.
[4] Ogi K, Takeda N, Prewo KM. Fracture process of thermally shocked discontinuous fiber-reinforced glass matrix composites under tensile loading. J Mater Sci 1997;32:6153–62.
[5] Hashin Z. Failure criteria for unidirectional fiber composites. J Appl Mech 1980;47:329–34.
[6] Hahn HT, Erikson JB, Tsai SW. Characterization of matrix/interface controlled strength of unidirectional composites, Fracture of composite materials. Dordrecht: Martinus Nijhoff, 1982 p. 197–214.
[7] Christensen RM, Swanson SR. Evaluation of a new failure criterion for fibrous composite materials. Mech Compos Mater 1988;AMD-92:63–68.
[8] Matzenmiller A, Schweizerhof K. Crashworthiness simulations of composite structures—a first step with explicit time integration. Munchen: CAD-FEM, 1991.
[9] Kutlu Z, Chang FK. Composite panels containing multiple through-the-width delaminations and subjected to compression. Part I: analysis. Compos Struct 1995;31:273–96.
[10] Meraghni F, Benzeggagh ML. Micromechanical modeling of matrix degradation in randomly discontinuous-fibre composites. Compos Sci Technol 1995;55:171–86.
[11] Meraghni F, Blakeman CJ, Benzeggagh ML. Effect of interfacial decohesion on stiffness reduction in a random discontinuous-fibre composite containing matrix microcracks. Compos Sci Technol 1996;56:541–55.
[12] Tohgo K, Weng GJ. A progress damage mechanics in particle-reinforced metal–matrix composites under high triaxial tension. J Engng Mater Techol 1994;116:414–20.
[13] Zhao YH, Weng GJ. A theory of inclusion debonding and its influence on the stress–strain relations of a ductile matrix composite. Int J Damage Mech 1995;4:196–211.
[14] Zhao YH, Weng GJ. Plasticity of a two-phase composite with partially debonded inclusions. Int J Plasticity 1996;12:781–804.
[15] Zhao YH, Weng GJ. Transversely isotropic moduli of two partially debonded composites. Int J Solids Struct 1997;34:493–507.
[16] Weibull W. A statistical distribution function of wide application. J Appl Mech 1951;18:293–7.
[17] Ju JW, Lee HK. A micromechanical damage model for effective elastoplastic behavior of ductile matrix composites considering evolutionary complete particle debonding. J Comput Meth Appl Mech Engng 2000;183:(in press).
[18] Lee HK, Simunovic S, A damage constitutive model of progressive debonding in aligned discontinuous fiber composites, Int J Solids Struct, 1999, submitted for publication.
[19] Lee HK. Three-dimensional micromechanical damage models for effective elastic and elastoplastic behavior of composite materials with inhomogeneities or microcracks, PhD Dissertation, University of California, LA, USA, 1998.
[20] Ju JW, Chen TM. Micromechanics and effective moduli of elastic composites containing randomly dispersed ellipsoidal inhomogeneities. Acta Mechanica 1994;103:103–21.
[21] Lagzdins A, Tamuzs V, Teters G, Kregers A. Orientational averaging in mechanics of solids. New York: Wiley, 1992.
[22] Halpin JC, Kardos JL. The Halpin–Tsai equations: a review. Polym Engng Sci 1976;16:344–52.
[23] Ju JW, Simo JC, Pister KS, Taylor RL. A parameter estimation algorithm for inelastic material models. In: Proceedings of the Second International Conference on Constitutive Laws for Engineering Materials: Theory and Application, 1987. p. 1233–40.
[24] Simo JC, Ju JW, Pister KS, Taylor RL. Assessment of cap model: consistent return algorithm and rate-dependent extension. J Engng Mech 1988;114:191–218.